REMOVING HARMONIC DISTORTION OF MEASUREMENTS OF A DEFOCUSING THREE-STEP PHASE-SHIFTING DIGITAL FRINGE PROJECTION SYSTEM

Zi-Xin XU and Yuk-Hee CHAN

Center for Multimedia Signal Processing
Dept. of Electronic and Information Engineering
The Hong Kong Polytechnic University
Email: ben.x.xu@connect.polyu.hk, enyhchan@polyu.edu.hk

ABSTRACT

Binary defocusing method was adopted in 3D profilometry as it allows real-time measurement and does not need to handle the luminance nonlinearity of a projector. Current patch-based binary fringe patterns are periodic and carry strong harmonic distortion as compared with the ideal sinusoidal fringe patterns, which affects the measuring performance remarkably. In this paper, we propose a framework for generating aperiodic fringe patterns based on optimized patches. The produced fringe patterns can significantly lower the noise floor and suppress the harmonic distortion in the constructed phase map. Accordingly, the achieved depth measuring performance can be significantly improved. Special care is also taken during the optimization of the patches in our framework such that the depth measuring performance is robust to fringe period and defocusing extent.

1. INTRODUCTION

Digital fringe projection technique[1] has been widely used in commercial 3D depth map acquisition in the past decades due to its simplicity, reliability and flexibility. When it is used, the projected fringe patterns impact the measurement quality directly. Phase-shifting sinusoidal patterns [2] are popular patterns used in digital fringe projection as they can provide pixel resolution measurement with reliable resistance to environmental noise. However, the measurement speed of the systems developed based on this technique is subject to the frame rates of a projector (typically <120 Hz). To release the speed bottleneck, square binary fringe patterns (SBM) were introduced by Su et. al. [3] and Lei et. al. [4] to produce sinusoidal-like fringe patterns with a properly defocused projector. These binary fringe patterns can be generated by simply toggling the mirrors of a digital micromirror device (DMD) and hence the frame rate can be increased dramatically. Another advantage of using binary fringe patterns is that they are not affected by the luminance nonlinearity of a projector, which eliminates one of the most annoying noise sources in 3D measurement. However, measurements based on SBM still suffer from their sensitivity to the extent of defocusing and the noise contributed by the high frequency harmonics of a binary square fringe pattern.

Various solutions have been proposed to reduce the unwanted high frequency harmonics induced by a square binary pattern. Early-stage proposals are mainly based on pulse width modulation (PWM) [5-11]. Recently, halftoning techniques have been extensively applied to produce high quality binary halftone patterns that can approximate the ideal sinusoidal patterns more closely after defocusing[12-19]. Their superiority over PWM-based solutions is due to the fact that halftoning is a two-dimensional process that can manipulate the noise more flexibly [20-22].

The optimization of the halftone patterns can be carried out in either intensity or phase domain. The former approach [13-15,17-19] tries to minimize the error between the defocused halftone and a

sinusoidal fringe pattern while the latter approach [16] tries to minimize the phase error achieved with the defocused halftone patterns. Since the quality of the depth measurement is determined by the phase error, the phase-based optimization tends to optimize the measurement quality directly while the intensity-based optimization does not. However, the performance of current phase-based optimization methods is more sensitive to the extent of defocusing which may not be controlled precisely in practical situations [15].

Sinusoidal fringe patterns are periodic. To provide flexibility and reduce the optimization effort, the optimization processes of recent proposals are generally patch-based [14,17-19]. In general, they optimize one single halftone patch of size $N_y \times (T/2)$ such that its defocused output is close to a patch of a sinusoidal fringe pattern, where T is the fringe period (in number of pixels) and N_y is an integer value. By tiling the patches and shifting the tiling results by $\pm 2T/3$ pixels, three full-size halftone patterns can be generated to approximate the ideal sinusoidal fringe patterns after being defocused. We have three observations on this common strategy as follows: (1) The tiling result must be periodic and hence it contains periodic noise with respect to the ideal sinusoidal fringe pattern. Consequently, the phase error contains harmonic distortion, which can mix with the phase variation contributed by the surface texture and reduce the measurement quality accordingly. (2) The shift must be an integer and hence the fringe period is bound to be an integer multiple of 3. (3) The phase error at a specific pixel, say (x,y), depends on three patch pixels, namely (x,y) and $(x,\mathrm{mod}(y+T\pm 2T/3,T))$, instead of patch pixel (x,y) itself, which introduces more constraint for the optimization process.

Although state-of-the-art researches have already reduced the phase error achieved by defocused binary patterns sharply, there still leave room for improvement, especially when fringe patterns of large period are applied during the measurement. It is obvious that the quality of a a quantized fringe pattern can be improved by increasing its quantization levels. We have introduced multilevel fringe patterns in [19] and demonstrated how they can improve the measurement efficiently. However, the defocused fringe patterns still suffer from the aforementioned problems due to the patch-based optimization process exploited to produce them.

To get an optimized halftone pattern the performance of which is robust to the amount of defocusing, conventional methods optimize halftone patterns under different conditions (e.g. different patch sizes [14,17-19] and different defocusing extent [14]) and then, from the optimized results, pick the one which is the most robust to defocusing conditions. This pick-the-best-from-the-available approach is passive to some extent and makes the optimization effort grow in multiples.

In this paper, we proposed a different optimization framework which generates multiple patches for tiling so that the periodicity of phase error can be effectively suppressed.

The contribution of this paper includes:

1) It is able to generate fringe patterns the produced phase error of which is close to aperiodic and carries almost no harmonic distortion.
2) It is capable to generate multilevel fringe patterns of arbitrary fringe period.
3) It releases a constraint for the optimization and theoretically it is able to achieve a better optimization result.
4) It takes proactive action to find optimized patches that are robust to defocusing extent.

The remainder of this paper is organized as follows. In Section 2, we briefly review the working principle of a three-step phase-shifting algorithm and the binary defocusing technique. In Section 3, we presented our idea of generating multi-level fringe patterns and our optimization procedures. Performance evaluation will be given in Section 4, and Section 5 presents the experimental results. Finally, a conclusion is provided in Section 6.

2. REVIEW OF BINARY DEFOCUSING THREE-STEP PHASE-SHIFTING ALGORITHM

Phase-shifting algorithms have been extensively used in 3D surface measurement because it can provide pixel-level accuracy and robustness. A simple three-step phase-shifting algorithm projects three sinusoidal fringe patterns, each of which has a phase shift of $2\pi/3$ from each other, onto the surface of the object to be measured. Accordingly, three phase-shifted fringe images, denoted as S_k for $k \in \{1,2,3\}$, can be captured with a high speed camera. Their intensity values at pixel (x, y) are given as:

$$S_1(x,y) = A + Mcos(\varphi(x,y) - 2\pi/3) \quad (1)$$

$$S_2(x,y) = A + Mcos\big(\varphi(x,y)\big) \quad (2)$$

$$S_3(x,y) = A + Mcos(\varphi(x,y) + 2\pi/3) \quad (3)$$

where A is the average intensity, M denotes the amplitude of intensity modulation, and $\varphi(x, y)$ symbolizes the pixel-wise phase to be solved. By solving the above three equations, we have:

$$\varphi(x,y) = \tan^{-1}\left(\sqrt{3}\frac{S_1(x,y)-S_3(x,y)}{2S_2(x,y)-S_1(x,y)-S_3(x,y)}\right) \quad (4)$$

Notably, the environmental noise can be eliminated by subtraction of different patterns. The solved phase from eqn. (4) is wrapped in range [-π, π]. After unwrapping $\varphi(x, y)$, one can obtain the depth information of the object.

A digital-light-processing (DLP) projector projects a gray level image with pulse width modulation (PWM)[23] and hence it takes time to project a gray-level pattern. To solve this problem, 8-bit sinusoidal patterns can be replaced with binary patterns such that the frame rate is only limited by the switching rate of the projection. Since switching can be super fast, it makes real-time 3D measurement feasible even though we still need to project 3 patterns onto the object being measured [24]. The issue is then how we can design a binary pattern that can approximate the original sinusoidal pattern well after being defocused under control.

Let B_k be the ideal binary pattern for approximating S_k for k={1,2,3}. In general, $B_k$can be obtained by minimizing the error in intensity domain as follows [15].

$$B_k = \min_B \| S_k - H \otimes B \|_2 \quad \text{for } k=\{1,2,3\} \quad (5)$$

where H is the blurring function that models the defocusing effect of the projector, B is a binary pattern having the same size of S_k, $\otimes$ denotes 2-D convolution, and $\|.\|_2$ symbolizes L2 norm. During the optimization process, H is generally modeled as a 2D Gaussian filter [12-19]. Patterns B_1, B_2 and B_3 can also be obtained by looking for three binary patterns that can minimize the L2 norm of the phase error resulted by replacing S_k with $H \otimes B_k$ in eqn. (4)[16].

As B_k is binary, optimizing B_k in either intensity or phase domain is a Non-deterministic Polynomial-time (NP) hard problem. Thus, optimization is usually realized by iteratively mutating pixels of B_k along raster scanning paths to find sub-optimal results [12-19].

3. PROPOSED FRINGE PATTERNS AND THEIR GENERATATION

3.1 Octa-level fringe patterns

A full color image can be separated into three color channels (R, G and B). Since the color channels are handled independently by a projector, one can produce three different binary patterns, one for each channel, for the projector to project a color fringe image X. The luminance channel of X, say L, can be generally determined as

$$L = 0.299B_R + 0.587B_G + 0.114B_B \quad (6)$$

where B_R, B_G and B_B are, respectively, the binary patterns for channels *R*, *G* and *B*. Let $B_c(x, y)$, where $c \in \{R,G,B\}$, be the intensity value of pixel (x, y) of pattern B_c. Since $B_c(x, y) \in \{0,1\}$ for all *c*, there are altogether $2^3 = 8$ possible intensity levels in *L*. In other words, if we project the color fringe image *X* onto the object and extract the luminance plane of the color image captured by the camera, it will be equivalent to projecting an octa-level fringe pattern onto the object directly.

Note that the actual luminance value associated with a particular color can vary among different projectors in practical situations. However, they can be acquired in the projector profile, or measured easily though a simple experiment before doing 3D measurements. Eqn. (6) can then be adjusted accordingly.

Since the proposed octa-level fringe patterns are actually produced by manipulating binary patterns in individual channels, it enjoys the following advantages:

1. Super fast measurement is supported because the frame rate can be as high as in the case when binary defocusing technique is used.
2. No gamma correction is required because only two extreme intensity levels are used in each color channel.
3. No color-shifting calibration is needed because there is no restriction on the exact intensity values of the 8 luminance levels.
4. Higher accuracy can be achieved because multilevel instead of binary fringe patterns are projected.

3.2 Objective function for optimization

Obviously, we need 3 octa-level fringe patterns, say L_1, L_2 and L_3, to approximate sinusoidal fringe patterns S_1, S_2 and S_3 respectively with the defocusing method such that the approximation error in phase domain is minimized. Besides the minimum error criterion, we would also like to achieve the following criteria: (1) the approximation performance is not sensitive to amount of defocusing, (2) the octa-level fringe patterns of any desirable sizes can be flexibly and easily constructed on site whenever necessary, and (3) the octa-level fringe patterns carry no low frequency harmonics and noise.

To achieve these goals, we propose to optimize two sets of three octa-level patch patterns, each of which is constructed with 3 binary patch patterns based on the color to luminance conversion defined in eqn. (6), by taking all the aforementioned criteria into account. Once they are obtained, by randomly tiling the two sets of patch patterns spatially, one can construct three aperiodic octa-level fringe patterns of any desirable size whenever necessary to do 3D shape measurement.

The success relies on how to optimize the two sets of octa-level patch patterns such that they can seamlessly connected to each other. Let $P_{(s,k)}$ be the k^{th} octa-level patch pattern of set $s \in \{0,1\}$, where $k \in \{1,2,3\}$. In our approach, for each *k*, we tile patch patterns $P_{(1,k)}$ and $P_{(2,k)}$ as shown in Figure 1 to form an octa-level pattern P_k, in which all possible neighboring combinations of $P_{(1,k)}$ and $P_{(2,k)}$ are included, and then optimize P_k for $k \in \{1,2,3\}$ together to minimize a cost function. Note that the occurrences of connection combinations $P_{(1,k)}P_{(1,k)}$, $P_{(1,k)}P_{(2,k)}$, $P_{(2,k)}P_{(1,k)}$ and $P_{(2,k)}P_{(2,k)}$ are identical in P_k and hence there should be no bias to favor a particular connection combination after the optimization.

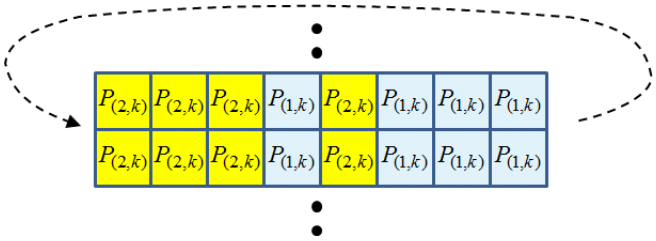

Fig.1 Constructing a circular connected octa-level pattern with two octa-level patch patterns for optimization.

Let H be a Gaussian low pass filter that models the defocusing effect of a projector. The phase map obtained with the defocused octa-level fringe patterns P_k for $k\in\{1,2,3\}$ is given as

$$\varphi_H(x,y)=\tan^{-1}\left(\frac{\sqrt{3}(H\otimes P_1(x,y)-H\otimes P_3(x,y))}{2H\otimes P_2(x,y)-H\otimes P_1(x,y)-H\otimes P_3(x,y)}\right) \tag{7}$$

where $H\otimes P_k(x,y)$ denotes the intensity value of the $(x,y)^{\text{th}}$ pixel of $H\otimes P_k$. The approximation error in phase domain can hence be defined as

$$\Delta\varphi=\sqrt{\Sigma_{x=1}^{M_1}\Sigma_{y=1}^{M_2}\left(\varphi(x,y)-\varphi_H(x,y)\right)^2/M_1M_2} \tag{8}$$

where $M_1\times M_2$ is the size of P_k. $\Delta\varphi$ is generally referred to as phase root mean square (rms) error and it is considered as a good measurement of approximation quality [12-19].

Different amount of defocusing should be taken into account during the optimization such that the approximation performance can be robust to it. In this paper, we model slight defocusing and severe defocusing, respectively, with a 5×5 Gaussian filter and an 11×11 Gaussian filter with their standard derivations equal to 1/3 of their sizes. Octa-level patterns P_k for $k\in\{1,2,3\}$ are optimized in parallel to minimize cost function

$$J=\Delta\varphi^5+\Delta\varphi^{11} \tag{9}$$

where $\Delta\varphi^t$ for $t=\{5,11\}$ denotes the $\Delta\varphi$ obtained when H is a $t\times t$ Gaussian filter used to model a specific amount of defocusing as mentioned earlier.

Recall that P_k is constructed with patch patterns as shown in Figure 1 and $P_{(s,k)}$ is actually the luminance plane of a color patch whose red, green and blue channels (denoted as $B_{R(s,k)}$, $B_{G(s,k)}$ and $B_{B(s,k)}$ hereafter) are all bi-level patches. Optimizing P_k for $k\in\{1,2,3\}$ is hence equivalent to solving the following optimization problem:

$$\min_{\substack{B_{R(s,k)},B_{G(s,k)},B_{B(s,k)}\\ \text{for } s\in\{1,2\} \text{ and } k\in\{1,2,3\}}} J \tag{10}$$

subject to the constraints that P_k is constructed with $P_{(s,k)}$ for s=1,2 as shown in Figure 1 and that

$$P_{(s,k)}=0.299B_{R(s,k)}+0.587B_{G(s,k)}+0.114B_{B(s,k)} \tag{11}$$

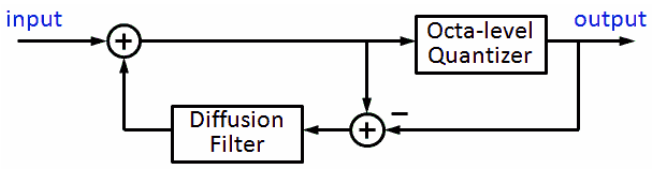

Fig. 2 Scheme of multilevel error diffusion

3.3 Optimization algorithm

As it is an NP hard problem, the optimization is realized as follows:

Let $C_{(s,k)}$ for $k\in\{1,2,3\}$ and $s\in\{1,2\}$ be 6 color patches of size $N_y\times N_x$ each, where N_x is fixed to be the fringe period of the target sinusoidal pattern. $C_{(s,k)}(x,y)$ denotes the color of pixel (x,y) in patch $C_{(s,k)}$. A color is represented as a vector belonging to set $\Omega=\{(r,g,b)|r,g,b\in\{0,1\}\}$, where r, g and b are the values of the red, green and blue components of the color. $P_{(s,k)}$ is the luminance plane of $C_{(s,k)}$.

Step 1. Initialization of $P_{(s,k)}$: Generate sinusoidal fringe patterns S_1, S_2 and S_3 of size $5N_y\times 8N_x$ each. Serpentine scan S_k for $k\in\{1,2,3\}$ separately. For each scanned pixel, quantize its intensity value to the nearest luminance value of the colors in Ω and then diffuse the quantization error with the diffusion filter suggested in [25] as shown in Figure 2. After the last pixel is processed, chop two connected $N_y\times N_x$ segments from the quantization result of S_k to form the initial versions of $P_{(1,k)}$ and $P_{(2,k)}$ respectively.

Step 2. Refining $P_{(1,k)}$: Raster scan patches $P_{(1,k)}$ for all k in parallel at the same pace and process their pixels sequentially according to the scanning order. Assume that the pixel location being scanned is (x,y). Let $P_{(1,k)}(x,y)$ be the luminance value of the $(x,y)^{\text{th}}$ pixel of $P_{(1,k)}$. Since $P_{(1,k)}$ is an octa-level pattern for each k, there are 8^3=512 possible value combinations of $P_{(1,k)}(x,y)$ for $k\in\{1,2,3\}$. For each combination, construct a candidate patch set $\Lambda=\{P_{(1,k)}|k=1,2,3\}$, in which all other pixels of $P_{(1,k)}$ remain the same as the most updated $P_{(1,k)}$, and tile $P_{(1,k)}\in\Lambda$ with the most updated $P_{(2,k)}$ as shown in Figure 1 to form a set of fringe patterns P_1, P_2 and P_3. Among all 512 candidate sets of $\{P_{(1,k)}|k=1,2,3\}$, the one used to construct the fringe patterns that minimizes J is the newly updated set of $P_{(1,k)}$ for all k. It continues until all pixels are scanned and processed.

Step 3. Refining $P_{(2,k)}$: Do step 2 again but exchange the roles of $P_{(1,k)}$ and $P_{(2,k)}$.

Step 4. Termination analysis: If the total improvement in steps 2 and 3 is larger than 0.01% in terms of J, go back to step 2. Otherwise the most updated $P_{(1,k)}$ and $P_{(2,k)}$ are considered as the optimal patches.

Step 5. Finalizing Fringe patterns: Randomly tile optimized patches $P_{(1,k)}$ and $P_{(2,k)}$ horizontally to form a patch row and then repeat the patch row vertically to form full-size octa-level fringe patterns L_k for $k\in\{1,2,3\}$ under the condition that L_1, L_2 and L_3 share the same random tiling pattern.

Notably, the optimization procedures are different from other patch-based optimization schemes (e.g. [14,17-19]) as follows:

1) We develop 2 sets instead of 1 set of patches such that one can construct full-size fringe patterns with them to eliminate periodic phase error and improve measurement quality.
2) We explicitly optimize 3 different patches for each set while the conventional approaches optimize only one single patch and then shift it by ±1/3 period to generate the other two patches, which removes the constraint that the fringe period must be an integer multiple of 3.
3) We explicitly take different defocusing conditions into account when constructing the objective function for optimization so that the optimized patterns are automatically robust to defocusing extent.

The optimization is time-consuming, but it is offline. Once the optimal patches $P_{(1,k)}$ and $P_{(2,k)}$ are determined, fringe patterns of different sizes can be easily generated by randomly tiling the patches.

4. SIMULATIONS

Simulations were carried out to evaluate the performance of the proposed octa-level fringe patterns. The performance is measured in terms of the phase error achieved with the defocused fringe patterns. For comparison, the phase errors achieved with the fringe patterns proposed in [16], [15], [14] and [19] were also evaluated. These fringe patterns are, respectively, referred to as *opt-p*, *opt-i*, *bpatch* and *cpatch* hereafter. The defocusing process was modeled as a 5×5 Gaussian filter with its standard derivation equal to 5/3 in our simulations unless else specified. Accordingly, fringe patterns *opt-p*, *opt-i*, *cpatch* were optimized for this defocusing condition while fringe patterns *bpatch* and the proposed were optimized to handle various defocusing conditions as in their original designs.

Fig. 3 shows the mean absolute phase errors achieved with different evaluated fringe patterns. The period of the target sinusoidal fringe pattern is 60 pixels. The x-axis corresponds to a line that cuts across a fringe pattern perpendicularly. The plot covers two fringe periods. The phase errors achieved with octa-level fringe patterns (*cpatch* and the proposed) are reduced significantly as compared with those achieved with binary fringe patterns (*opt-p*, *opt-i* and *bpatch*). Unlike *bpatch* and *cpatch*, the proposed fringe patterns do not introduce periodic phase errors though they are all patch-based.

Fig.4 shows the power spectral densities of the phase errors achieved with different fringe patterns. The spectrum associated with *opt-p* is not included because it is similar to the one associated with *opt-i*. One can see the strong harmonic distortion in the plots of *bpatch* and *cpatch*. In contrast, the phase errors associated with *opt-i* and ours are more like white noise. The noise floor of ours is much lower than *opt-i* and *bpatch.*

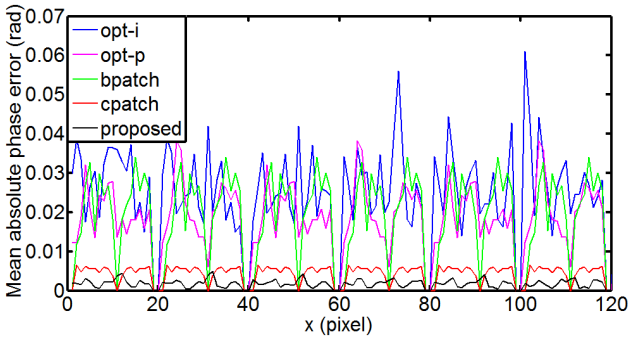

Fig. 3 Mean absolute phase errors achieved with *opt-i*, *opi-p*, *bpatch*, *cpatch* and the proposed fringe patterns

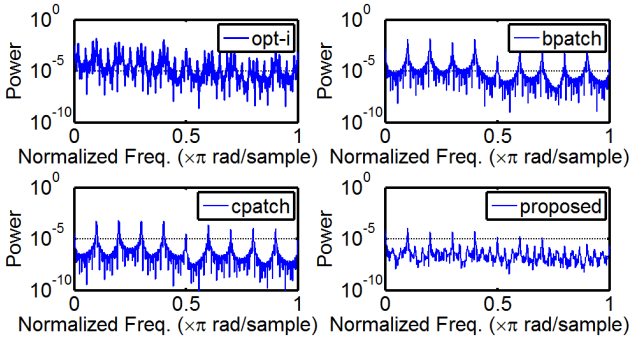

Fig. 4 Power spectral densities of the phase errors associated with *opt-i*, *bpatch*, *cpatch* and the proposed fringe patterns

Fig. 5(a) shows the performance achieved with the evaluated fringe patterns in terms of phase rms error when their fringe periods vary from 30 to 120 pixels. Note that the fringe periods of other evaluated fringe patterns must be an integer multiple of 3 while ours do not have this limitation. One can see that the proposed fringe patterns perform well consistently when the fringe period changes. As expected, octa-level fringe patterns (*cpatch* and the proposed) performs better than binary ones (*opt-i*, *opi-p*, *bpatch*). The difference between *cpatch* and the proposed fringe patterns shows the advantage of using fringe patterns with less harmonic distortion.

The same set of fringe patterns evaluated to produce Fig. 5(a) were also evaluated under different defocusing conditions to investigate whether their performance is robust to defocusing. In our study, different amount of defocusing is achieved by filtering the fringe patterns with a $t \times t$ Gaussian filter with its standard derivation equal to $t/3$, where $t \in \{7,9,11\}$. The simulation results shown in Figs. 5(b)-(d) show that the performances of the proposed fringe patterns are robust to defocusing.

Fig. 6 shows some simulation data for measuring a three-dimensional surface. In the simulation, the fringe period of all fringe patterns is 60 pixels, and a simple phase unwrapping algorithm [26] is exploited. The defocusing process is modeled as a 5×5 Gaussian filter with standard derivation equal to 5/3. Obviously, the unwrapped phase maps obtained with octa-level fringe patterns are more accurate. Note that the gain is at no cost to a certain extent as only a binary pattern is manipulated in each color channel. After suppressing the harmonic distortion, the unwrapped phase map obtained with our fringe patterns can preserve the parallel ridges much better than the one obtained with *cpatch*.

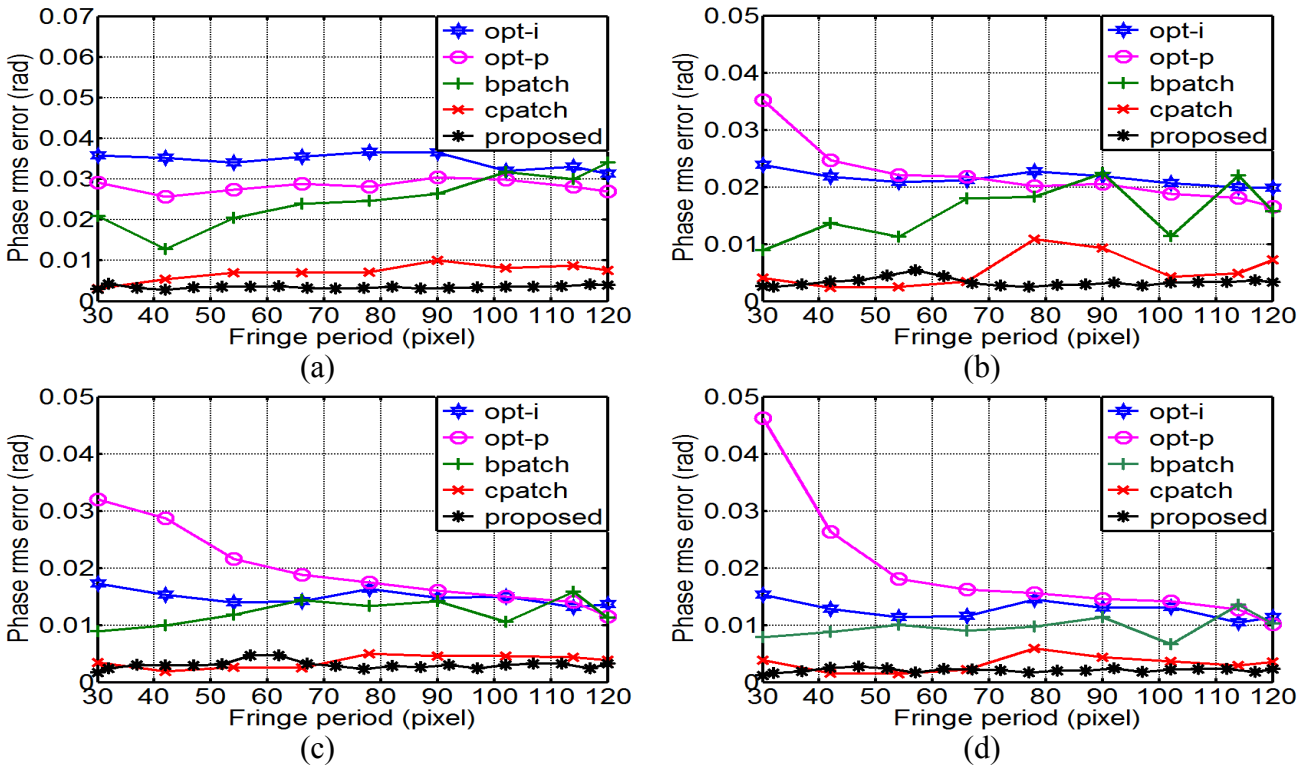

Fig. 5 Simulated phase rms errors achieved with different fringe patterns of different fringe periods when defocusing levels are simulated by Gaussian filter of size (a) 5×5, (b) 7×7, (c) 9×9, and (d) 11×11 pixels

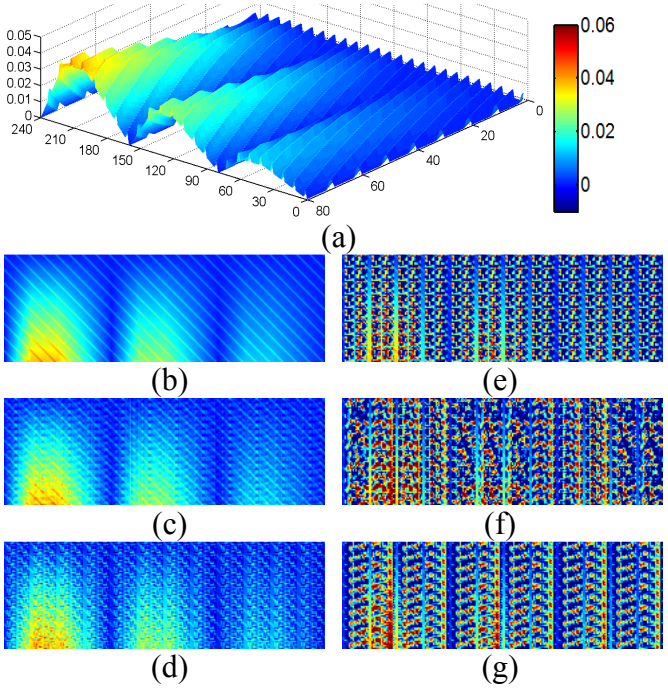

Fig.6 Simulation results for measuring an object. (a) 3D plot of the object; (b) ideal unwrapped phase map; and unwrapped phase maps obtained with (c) ours, (d) *cpatch*, (e) *bpatch*, (f) *opt-i* and (g) *opt-p*.

5. EXPERIMENTS

A real 3D shape measurement system was set up to measure the object shown in Fig. 7(a). The system consists of a DLP projector (Texas MP723) and a CCD camera (Canon 400D). The size of a projected fringe pattern is 1024×768 pixels. The fringe period is 18 pixels. The reference plane is placed around 0.5 meters away from the projector.

Fig. 7(b) shows the depth map (unit in cm) obtained with the grayscale nine-step phase-shifting algorithm[2]. To tackle the gamma nonlinearity of the projector, active gamma correction [27] was done to produce the grayscale sinusoidal fringe patterns. The depth map is used as the reference depth map for comparison.

Figs. 7(c), 7(d), 7(e) and 7(f) show, respectively, the depth maps obtained with *bpatch, opt-i, cpatch* and the proposed aperiodic multilevel fringe patterns. All of them are similar to the reference depth map shown in Fig. 7(b). However, their rms depth errors are, respectively, 0.0324 cm, 0.0334 cm, 0.0252 cm and 0.0175 cm. The proposed fringe patterns perform better than binary patterns. Remind that no gamma calibration for the projector is required and real-time realization is feasible when the proposed method is used.

6. CONCLUSIONS

In this paper, we propose a framework for generating aperiodic octa-level fringe patterns for real time 3D shape measurement. As compared with conventional patch-based frameworks, it is able to produce fringe patterns of arbitrary fringe period and higher gray-level resolution without introducing harmonic distortion. The achieved depth measuring performance can be significantly improved and is robust to fringe period and defocusing extent. The gain is almost at no cost because a measuring system exploiting the proposed octa-level fringe patterns shares the same advantages with the systems using binary fringe patterns.

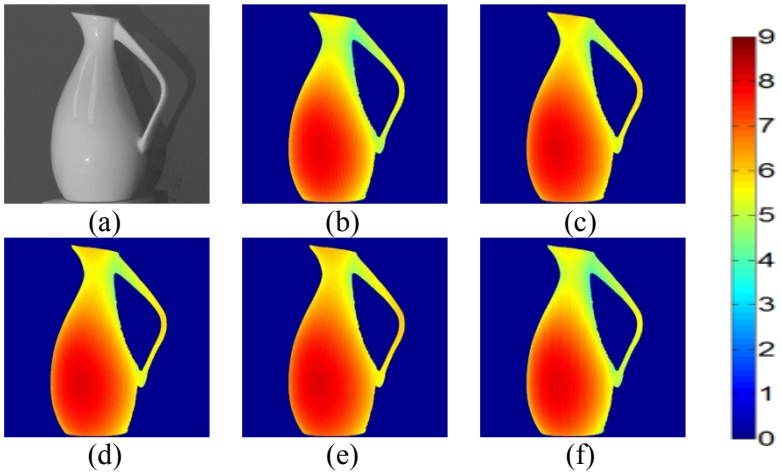

Fig. 7 Experimental results for measuring a jug: (a) object and the depth maps obtained with (b) sinusoidal fringe patterns, (c) *bpatch,* (d) *opt-i,* (e) *cpatch,* and (f) our proposed aperiodic fringe patterns.

ACKNOWLEDGMENTS

This work was supported by Multimedia Signal Processing Center and The Hong Kong Polytechnic University under Grant number G-YBAN.

REFERENCES

[1] Gorthi S, Rastogi P. Fringe projection techniques: whither we are? Opt Lasers Eng 2010;48:133–40.
[2] Malacara D. Optical shop testing. 3rd ed. New York: Wiley; 2007.
[3] Su X-Y, Zhou W-S, von Bally G, Vukicevic D. Automated phase-measuring profilometry using defocused projection of a Ronchi grating. Opt Commun 1992;94:561–73.
[4] Lei S, Zhang S. Flexible 3-D shape measurement using projector defocusing. Opt Lett 2009;34:3080.
[5] Ayubi G a, Ayubi J a, Di Martino JM, Ferrari J a. Pulse-width modulation in defocused three-dimensional fringe projection. Opt Lett 2010;35:3682–4.
[6] Wang Y, Zhang S. Optimal pulse width modulation for sinusoidal fringe generation with projector defocusing. Opt Lett 2010;35:4121.
[7] Ayubi GA, Ferrari JA. Optimal pulse-width modulation for sinusoidal fringe generation with projector defocusing: comment. Opt Lett 2011;36:808.
[8] Zuo C, Chen Q, Feng S, Feng F, Gu G, Sui X. Optimized pulse width modulation pattern strategy for three-dimensional profilometry with projector defocusing. Appl Opt 2012;51:4477.
[9] Zuo C, Chen Q, Gu G, Ren J, Sui X, Zhang Y. Optimized three-step phase-shifting profilometry using the third harmonic injection. Opt Appl 2013;43.
[10] Zuo C, Chen Q, Gu G, Feng S, Feng F, Li R, et al. High-speed three-dimensional shape measurement for dynamic scenes using bi-frequency tripolar pulse-width-modulation fringe projection. Opt Lasers Eng 2013;51:953–60.
[11] Wang Y, Zhang S. Comparison of the squared binary, sinusoidal pulse width modulation, and optimal pulse width modulation methods for three-dimensional shape measurement with projector defocusing. Appl Opt 2012;51:861.
[12] Wang Y, Zhang S. Three-dimensional shape measurement with binary dithered patterns. Appl Opt 2012;51:6631.
[13] Lohry W, Zhang S. Genetic method to optimize binary dithering technique for high-quality fringe generation. Opt Lett 2013;38:540.
[14] Sun J, Zuo C, Feng S, Yu S, Zhang Y, Chen Q. Improved intensity-optimized dithering technique for 3D shape measurement. Opt Lasers Eng 2015;66:158–64.
[15] Dai J, Li B, Zhang S. Intensity-optimized dithering technique for three-dimensional shape measurement with projector defocusing. Opt Lasers Eng 2014;53:79–85.
[16] Dai J, Zhang S. Phase-optimized dithering technique for high-quality 3D shape measurement. Opt

Lasers Eng 2013;51:790–5. doi:10.1016/j.optlaseng.2013.02.003.
[17] Dai J, Li B, Zhang S. High-quality fringe pattern generation using binary pattern optimization through symmetry and periodicity. Opt Lasers Eng 2014;52:195–200.
[18] Li X, Zhang Z, Yang C. High-quality fringe pattern generation using binary pattern optimization based on a novel objective function. Opt - Int J Light Electron Opt 2016;127:5322–7.
[19] Xu Z-X, Chan Y-H. Optimized multilevel fringe patterns for real-time 3D shape measurement with defocused projector. 2015 IEEE Int. Conf. Image Process., IEEE; 2015, p. 2730–4.
[20] Lau DL, Arce GR. Modern digital halftoning. 2rd ed. CRC Press; 2008.
[21] Fung Y-H, Chan Y-H. Tone-dependent noise model for high-quality halftones. J Electron Imaging 2013;22:023004.
[22] Fung Y-H, Chan Y-H. Tone-dependent error diffusion based on an updated blue-noise model. J Electron Imaging 2016;25:013013.
[23] Hornbeck LJ. Digital Light Processing for high-brightness high-resolution applications. International Society for Optics and Photonics; 1997, p. 27–40.
[24] Karpinsky N, Hoke M, Chen V, Zhang S. High-resolution, real-time three-dimensional shape measurement on graphics processing unit. Opt Eng 2014;53:024105.
[25] Floyd RW, Steinberg L. Adaptive algorithm for spatial greyscale 1976;17:75–7.
[26] Ghiglia DC, Pritt MD. Two-dimensional phase unwrapping : theory, algorithms, and software. Wiley; 1998.
[27] Zhang S. Active versus passive projector nonlinear gamma compensation method for high-quality fringe pattern generation. International Society for Optics and Photonics; 2014, p. 911002.